

Article

# Toluene Steam Reforming over Ni/CeZrO<sub>2</sub>—The Influence of Steam to Carbon Ratio and Contact Time on the Catalyst Performance and Carbon Deposition

Agata Łamacz 

Department of Engineering and Technology of Chemical Processes, Wrocław University of Science and Technology, Gdańska 7/9, 50-344 Wrocław, Poland; agata.lamacz@pwr.edu.pl

**Abstract:** The formation of tars during coal or biomass gasification is a serious issue resulting in decreasing efficiency of the process and increased maintenance costs. The decomposition of tars can be conducted via catalytic steam reforming that enriches the produced gas in hydrogen. Nevertheless, the catalyst should be characterized by high activity, stability, and resistance towards carbon deposition. Ceria-zirconia supported nickel (Ni/CeZrO<sub>2</sub>) is a very good candidate to catalyze tar removal—Ni is an active phase for reforming reactions, while CeZrO<sub>2</sub> provides the active sites that play important roles in protecting the catalyst from carbon deposition. Ni/CeZrO<sub>2</sub> shows high activity in the steam reforming of model tar compounds. In this paper, its performance in the steam reforming of toluene and carbon deposition is discussed considering the changing parameters of the reaction: the temperature, steam to carbon ratio, and the contact time.

**Keywords:** steam reforming; toluene; carbon deposits; ceria-zirconia; nickel



**Citation:** Łamacz, A. Toluene Steam Reforming over Ni/CeZrO<sub>2</sub>—The Influence of Steam to Carbon Ratio and Contact Time on the Catalyst Performance and Carbon Deposition. *Catalysts* **2022**, *12*, 219. <https://doi.org/10.3390/catal12020219>

Academic Editors: Monika Motak, Xiangtong Meng and Xiong Zhang

Received: 14 January 2022

Accepted: 5 February 2022

Published: 15 February 2022

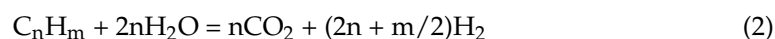
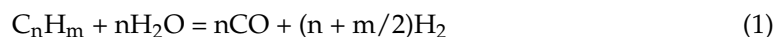
**Publisher's Note:** MDPI stays neutral with regard to jurisdictional claims in published maps and institutional affiliations.



**Copyright:** © 2022 by the author. Licensee MDPI, Basel, Switzerland. This article is an open access article distributed under the terms and conditions of the Creative Commons Attribution (CC BY) license (<https://creativecommons.org/licenses/by/4.0/>).

## 1. Introduction

Both coal and biomass gasification are accompanied by the formation of tars that negatively influence the efficiency and total cost of the process. The most widely used techniques for tar removal are thermal cracking, steam reforming, and mechanical separation [1]. The latter, however efficient, has a significant negative impact on the environment. The catalytic steam reforming of tar is a very attractive approach allowing for tar decomposition, and it has been intensively studied using model compounds, such as toluene, benzene, or naphthalene [2–6]. The main reactions occurring during steam reforming process are steam reforming (SR) (Equation (1)), total oxidation (Equation (2)), water gas shift (WGS) (Equation (3)), and coking (Equation (4)). Besides WGS, all reactions are endothermic. The formation of CO<sub>2</sub> in WGS is favored at low temperatures while the reverse reaction (RWGS), which yields CO, is privileged at high temperatures.



The deposition of carbon on the catalyst during the steam reforming process is currently a significant technological challenge. It negatively influences the performance of the catalyst by blocking or destroying the active sites. The catalytic reforming of various hydrocarbons (e.g., methane, ethane, ethanol, propane, toluene, and naphthalene) and their derivatives has been extensively studied by several researchers [7–11]. These studies in most concentrate on minimizing carbon formation and thus, catalyst deactivation.

There are two main research blocks engaged in reducing carbon deposition during reforming reactions. The first one deals with the selection of reaction conditions, e.g., temperature, steam to carbon ratio (S/C) in the case of steam reforming (SR), CO<sub>2</sub> to carbon ratio (CO<sub>2</sub>/C) for dry reforming (DR), and oxygen to carbon ratio (O/C) for the reaction of partial oxidation (POX). Studies on the effect of water vapor on the performance of Ni/Al<sub>2</sub>O<sub>3</sub> and Ni-Mo/Al<sub>2</sub>O<sub>3</sub> in the SR of hydrocarbons revealed that the presence of H<sub>2</sub> inhibits nickel oxidation by H<sub>2</sub>O but does not inhibit the oxidation of Mo. Therefore, due to its higher oxygen content, Ni-Mo/Al<sub>2</sub>O<sub>3</sub> was found to be more resistant to carbon deposition during SR than Ni/Al<sub>2</sub>O<sub>3</sub> [12]. Rh/MgO-Al<sub>2</sub>O<sub>3</sub> has been found to be highly active and stable in methane steam reforming. Moreover, it exhibited very good coke resistance, even under S/C = 1 [13]. Studies on the steam reforming of m-cresol over Ni/MgO revealed that sufficient water feeding can favor carbon conversion from solid and liquid to a gaseous phase. However, high coke formation was noticed to occur at temperatures ranging from 575 to 900 °C [14]. The increase in H<sub>2</sub>O content in the feed also resulted in increased hydrocarbon conversion. Kim et al. [15] observed that CH<sub>4</sub> conversion over Ni/Al<sub>2</sub>O<sub>3</sub> and Ni/MgOAl<sub>2</sub>O<sub>4</sub> catalysts was 84% when the reaction was carried out at S/C = 1 and increased to 97% at S/C = 2. The impact of S/C was even more pronounced in the case of Ni/CeO<sub>2</sub>, over which CH<sub>4</sub> conversion increased from 40% at S/C = 1 to 89% at S/C = 2. Toluene, considered a model tar compound, was converted in the SR reaction over Ni/Al<sub>2</sub>O<sub>3</sub> [16]. The catalyst showed the highest toluene conversion and hydrogen yield with the lowest coke deposition at elevated temperatures (above 800 °C). It was found that the rate of carbon deposition over a Ni/Al<sub>2</sub>O<sub>3</sub> catalyst increased as GHSV increased. A higher S/C ratio increased the total conversion of toluene and promoted coke gasification.

The second research block concerns the catalyst design by modification of its physico-chemical properties, e.g., by introducing appropriate additives, such as potassium [17] or molybdenum [12,18,19] and thus increasing the basicity of the catalyst.

The application of supports with unique redox properties, like rare earth metal oxides, has been also studied [20,21]. Laosiripojana and Assabumrungrat [22] studied the steam reforming of methane (SRM) over a Ni catalyst supported on ceria-zirconia (Ni/CeZrO<sub>2</sub>) at 650–900 °C. The resistance of Ni/CeZrO<sub>2</sub> to carbon deposition was much higher than in the case of Ni/Al<sub>2</sub>O<sub>3</sub> at the same operating conditions. Nevertheless, a small catalyst deactivation was noticed. High surface area ceria (HAS-CeO<sub>2</sub>) and CeZrO<sub>2</sub> with a Ce/Zr ratio of 3/1 were found to be very good supports for Ni catalysts for methane steam reforming.

The Ni-CeO<sub>2</sub>/SBA-15 catalysts with a different content of Ni-CeO<sub>2</sub> phase were studied in toluene steam reforming by Tao et al. [23]. The catalysts exhibited good toluene conversion and stability and were resistant to coke deposition. Toluene conversion increased with CeO<sub>2</sub> loading and the S/C ratio up to 3. The best performance was noticed for Ni-CeO<sub>2</sub>(3 wt.%)/SBA-15 at 850 °C and S/C = 3.

Zhou et al. [24] obtained a series of three-dimensional ordered macroporous Ni-Pt/Ce<sub>1-x</sub>Zr<sub>x</sub>O<sub>2</sub> using a colloidal crystal template method. Thanks to its textural properties, a higher concentration of oxygen vacancies, and better reducibility compared to their non-porous counterparts, those catalysts exhibited excellent catalytic performance at temperatures as low as 500 °C. They also showed good stability and a carbon deposition rate of only 1.7 mg/g<sub>cat</sub>/h during a 30 h test at 600 °C.

The Ni/ZrO<sub>2</sub> catalysts were studied in toluene, methane, and toluene/methane steam reforming by Silveira et al. [25]. The catalyst's deactivation caused by carbon deposition depended strongly on the composition of the reaction feed and the crystallographic features of the catalysts. It was found that more carbon deposited on the catalysts containing tetragonal ZrO<sub>2</sub>, which showed higher acidity and catalyzed oligomerization of toluene molecules, whereas the monoclinic ZrO<sub>2</sub> contained more hydroxyl groups and was more resistant to carbon build-up.

The formation of carbon deposits over nickel catalysts was studied by [22,26,27]. It was reported that the support/s modifications and the size of Ni crystallite have significant effects on carbon formation. It is also well known that carbon deposition on the metal-

supported catalyst is significantly influenced by the metal-support interaction (MSI), which is associated with the method of catalyst preparation, the temperature of calcination, and its pre-treatment [28].

There are different types of carbon deposits on the catalyst surface. The most popular are pyrolytic carbon, whisker carbon, and encapsulating carbon. The formation of pyrolytic carbon takes place when the temperature is increased to over 600 °C while whisker carbon is usually produced at 500–600 °C [14,28–32]. The formation of whisker carbon during biomass steam reforming was studied by Kihlman et al. [33]. The authors found that carbon deposition over Ni can be significantly reduced when the catalyst is doped with Ca. Moreover, the beneficial impact of the H<sub>2</sub>S introduction, which has poisoned the active sites for C deposition, was observed. The “whisker carbon-free” operating temperature of the biomass steam reforming depended on the following factors: the composition of biomass, the concentration of the unsaturated C<sub>2+</sub> hydrocarbons which rapidly form C deposits, the concentration of H<sub>2</sub>S in the dry biomass gasification gas, and the S/C ratio.

Filamentous carbons, such as carbon nanotubes (CNTs) have been identified on the surfaces of catalysts spent in SR reactions. In recent years, several works have been published on the intentional production of CNTs (together with H<sub>2</sub>) during steam reforming processes. Those works relate to the SR of formaldehyde over NiO/MoO<sub>3</sub> at 300–600 °C [34], the SR of ethanol over Ni/CaO at 600 °C [35], or the “pyrolysis-catalytic” SR of used tires over Ni/Al<sub>2</sub>O<sub>3</sub> at 900 °C [36]. CNTs are often produced in the reaction of CO disproportionation or CH<sub>4</sub> dehydrogenation. However, arenes such as benzene or naphthalene are also feasible materials for obtaining CNTs [37]. Before building up a CNT, those hydrocarbons are believed to form small polycyclic arenes (PCAs) that undergo condensation. For example, Tian et al. [38,39] who studied CNT formation from benzene, reported that PCAs were built from the benzene blocks. Their observations were proved by Zhang et al. [37]. The growth mechanism of CNTs from a benzene precursor over a nickel catalyst was also studied by Feng et al. [40] using the density functional theory (DFT). Multiwalled carbon nanotubes (MWNTs) and nanofilaments were produced in supercritical toluene by Lee et al. [41] using ferrocene, or prefabricated Fe or FePt nanocrystals. According to this study, efficient MWNT formation requires temperatures in the 550–625 °C range. Moreover, the formation of carbon nanotubes was promoted over smaller particles (<30 nm diameter), while the larger particles produced carbon nanofilaments with disordered graphitic cores.

The activity of the catalyst in the steam reforming of tars (being partly composed of aromatic hydrocarbons) may be deteriorated owing to the formation of structural carbon deposits. Hence, to reduce the risk of catalyst deactivation, one must pay attention to its chemical composition and morphology. In this work, Ni/CeZrO<sub>2</sub>, which is characterized by very good activity in reforming reactions and shows high resistance towards deactivation by carbon species, was studied in toluene steam reforming. The performance of this catalyst, especially regarding toluene conversion, hydrogen production, and carbon deposition, was investigated during tests conducted under different steam excesses and various contact times. The participation of reactions occurring in parallel to steam reforming, i.e., WGS and H<sub>2</sub>O dissociation, was also examined.

## 2. Results and Discussion

### 2.1. Catalytic Runs of Toluene Steam Reforming over CeZrO<sub>2</sub> and Ni/CeZrO<sub>2</sub>

The results of the catalytic runs of steam reforming of toluene (SRT) over CeZrO<sub>2</sub> and Ni/CeZrO<sub>2</sub> conducted at S/C = 2.4 and t<sub>c</sub> = 0.36 s are presented in Table 1, which shows that toluene converts mainly to CO and CO<sub>2</sub>, with some insignificant transformation to benzene in the reaction of steam dealkylation (Equation (5)). Some works reported the formation of CH<sub>4</sub> during SRT [29]; nevertheless, it was not detected in this study. Methane can be produced in the reaction of toluene hydrodealkylation (Equation (6)) and as an important precursor for carbon deposition (Equation (7)), its formation during SRT is unwanted. In the present work, the only by-product detected by GC and GC-MS in the product gas was benzene. From Table 1, it can be seen that toluene conversion to benzene

is higher over CeZrO<sub>2</sub> than over Ni/CeZrO<sub>2</sub>, and for both, it decreases with the increase of the reaction temperature. The selectivity to benzene is much higher for CeZrO<sub>2</sub> than for Ni/CeZrO<sub>2</sub>. Bion et al. [42], who studied toluene steam dealkylation over Al<sub>2</sub>O<sub>3</sub>-supported Rh, Pd, Pt, Ni, Co, Ru, and Ir, found out that contrary to the SRT reaction, toluene steam dealkylation is insensitive to the nature of the metal and the structure of the catalyst (that is also changing due to carbon deposition). However, toluene steam dealkylation was found to be very sensitive to the nature of the support. For example, for metal catalysts supported on alumina, silica, or chromium oxide, toluene dealkylation to benzene (that immediately desorbs to the gas phase) and CH<sub>x</sub> species takes place on the metal active sites, while H<sub>2</sub>O is activated on the support sites. In the next step, the OH groups diffuse from the support to the CH<sub>x</sub> (remaining on the metal sites) and oxidize them to CO and H<sub>2</sub>. According to Wang and Gorte [43], toluene steam dealkylation is not occurring on the CeO<sub>2</sub>-supported Pt and Pd catalyst. Nevertheless, in the present work, it is shown that some small amounts of benzene are formed during SRT over CeZrO<sub>2</sub> alone, but production of this hydrocarbon is significantly decreased in the presence of Ni.

**Table 1.** The results of the catalytic runs of toluene steam reforming carried out in isothermal conditions on CeZrO<sub>2</sub> and Ni/CeZrO<sub>2</sub> catalysts (S/C = 2.4, t<sub>c</sub> = 0.36 s, TOS at each temperature was 4 h).

Catalyst	T (°C)	C <sub>7</sub> H <sub>8</sub> Conversion to CO/CO <sub>2</sub> (%)	C <sub>7</sub> H <sub>8</sub> Conversion to C <sub>6</sub> H <sub>6</sub> (%)	Selectivity to C <sub>6</sub> H <sub>6</sub> (%)	H <sub>2</sub> Yield (%)
CeZrO <sub>2</sub>	500	1	1.51	60.1	>1
	600	22	1.89	7.9	30
	700	49	2.1	4.1	51
	800	73	0	0	64
	900	78	0	0	65
Ni/CeZrO <sub>2</sub>	400	21	-	-	36
	450	36	0.15	0.4	47
	500	64	0.25	0.4	68
	600	88	0.21	0.2	86
	700	98	0	0	80
	800	97	0	0	81
900	99	0	0	85	

In general, the performance of Ni/CeZrO<sub>2</sub> is much better than of CeZrO<sub>2</sub>—especially at temperatures up to 700 °C, which is owing to the presence of the Ni active phase. But it must be pointed out that CeZrO<sub>2</sub> alone exhibits relatively good performance in SRT, especially at elevated temperatures (800 and 900 °C). Thus, it is evident that ceria-zirconia provides some catalytic activity to the Ni/CeZrO<sub>2</sub> system. The reduced ceria (Ce<sup>3+</sup>) is responsible for H<sub>2</sub>O dissociation, while Ce<sup>4+</sup> is the site for toluene dealkylation to CH<sub>x</sub> and C<sub>6</sub>H<sub>6</sub>, followed by the hydrogenation of the latter to a cyclic ring that breaks to form CH<sub>x</sub>. The CH<sub>x</sub> species are dehydrogenated to H<sub>2</sub> and active carbon species that are oxidized to CO using the oxygen from CeO<sub>2</sub> (supplied by dissociating H<sub>2</sub>O molecules). In the Ni/CeZrO<sub>2</sub> catalyst, ceria-zirconia is considered as the oxygen source that is used for the oxidation of carbon species on the Ni, rather than as the active site for toluene activation. Whereas the nickel species Ni<sup>0</sup> and Ni<sup>x+</sup> are responsible for C<sub>7</sub>H<sub>8</sub> and H<sub>2</sub>O dissociation, respectively.



## 2.2. The Influence of S/C on the Ni/CeZrO<sub>2</sub> Activity in SRT

The results of the catalytic runs conducted at S/C = 1, 1.2, 2.4, and 4 (Figure 1) prove that the increase in H<sub>2</sub>O content in the reaction mixture has a positive influence on C<sub>7</sub>H<sub>8</sub> conversion. The most important effect of S/C on hydrocarbon conversion is observed at lower temperatures. For example, at 420 °C, toluene conversion is only 30% for S/C = 1 and 96% for S/C = 4. It should be noticed also that at a high steam content, the conversion of toluene is almost constant in the whole range of applied temperatures (Figure 1d). A slight increase in S/C (from 1 to 1.2) does not influence toluene conversion; however, it enables to improve the suppression of carbon deposits and protect the catalyst from deactivation. A further increase in H<sub>2</sub>O concentration in the feed (Figure 1c,d) results in a visible increase in hydrocarbon conversion. For example, at a temperature as low as 420 °C, toluene conversion is 66% and 96% for SC = 2.4 and 4, respectively. At an increased steam excess, the Ni/CeZrO<sub>2</sub> catalyst shows very good performance in SRT even at lower temperatures (500–600 °C). For S/C = 2.4, toluene conversion of ca. 90% is observed from 600 °C, while for S/C = 4, over 99% toluene conversion is noticed even from 500 °C.

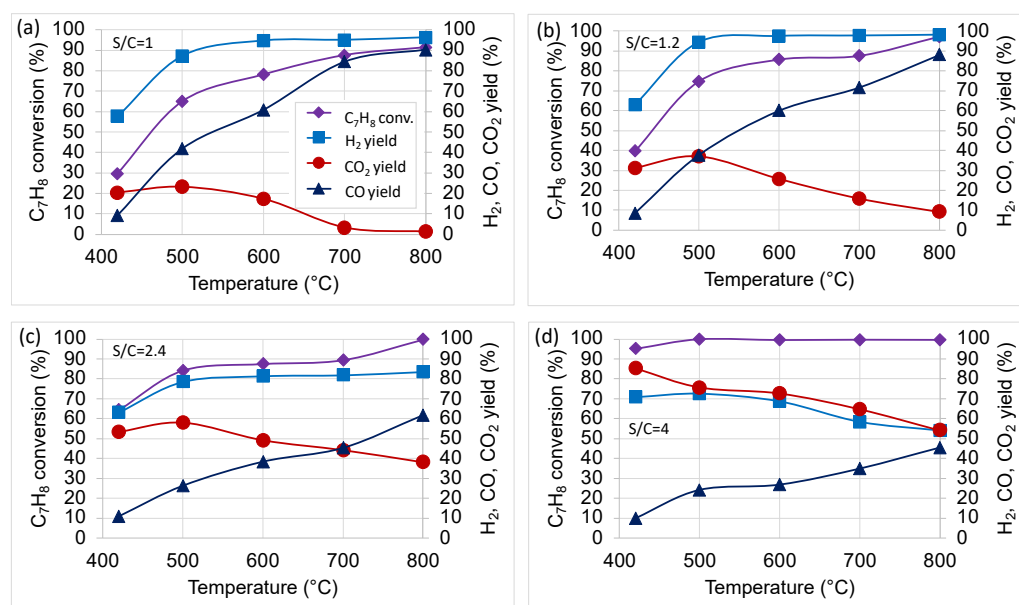


**Figure 1.** The evolution of C<sub>7</sub>H<sub>8</sub> conversion and CO, CO<sub>2</sub>, and H<sub>2</sub> yields during catalytic runs of SRT carried out on Ni/CeZrO<sub>2</sub> at  $t_c = 0.36$  s and under the S/C ratio of 1 (a), 1.2 (b), 2.4 (c), and 4 (d). Time-on-stream at each temperature was 24 h.

It can be seen from Figure 1 that the yields of CO and CO<sub>2</sub> also depend on the applied S/C ratio. The production of CO<sub>2</sub> during catalytic runs of SRT is ascribed to the occurrence of the WGS reaction (Equation (3)), which is thermodynamically favored at lower temperatures. The CO<sub>2</sub> formation during catalytic runs increases with increasing S/C. The higher the H<sub>2</sub>O concentration in the feed, the more CO<sub>2</sub> is detected at the reactor's outlet. For S/C = 4, the CO<sub>2</sub> formation predominates in the whole range of applied temperatures.

The GC-MS analyses at the reactor's outlet during tests carried out at S/C = 1 and 2.4 (Table 2) revealed that in the 420–600 °C range, the SRT over Ni/CeZrO<sub>2</sub> produces small amounts of benzene. It is observed that the formation of benzene is inversely proportional to the temperature and steam excess. No benzene is produced at 700–900 °C for S/C = 1 and 2.4. Moreover, benzene was not present in the product gas (in the whole range of temperatures) when S/C = 4. Doumani [44] reported that during toluene dealkylation at ca. 560 and 620 °C, the conversion to benzene decreased with an increasing H<sub>2</sub>O/C<sub>7</sub>H<sub>8</sub> molar ratio. The effect of H<sub>2</sub>O/C<sub>7</sub>H<sub>8</sub> was also found to be more important at higher temperatures.

**Table 2.** The conversion of toluene to benzene and benzene selectivity during catalytic runs of SRT over Ni/CeZrO<sub>2</sub> at  $t_c = 0.36$  s, and S/C = 1 and 2.4, determined after 24 h time-on-stream at each T.

T (°C)	C <sub>7</sub> H <sub>8</sub> Conversion to C <sub>6</sub> H <sub>6</sub> (%)		Selectivity to C <sub>6</sub> H <sub>6</sub> (%)	
	S/C = 1	S/C = 2.4	S/C = 1	S/C = 2.4
420	2.1	0.6	7.2	0.9
500	1.6	0.5	2.5	0.6
600	1.3	0.2	1.7	0.2

The results presented in this paper revealed that the effect of the S/C ratio on the performance of Ni/CeZrO<sub>2</sub> in toluene steam reforming is more important at temperatures below 600 °C. At low temperatures, high H<sub>2</sub>O excess inhibits catalyst deactivation caused by carbon deposition and enriches the product gas in hydrogen owing to the occurrence of WGS and H<sub>2</sub>O dissociation [43]. However, a high content of H<sub>2</sub>O may lead to catalyst sintering, finally causing a decrease of its activity.

According to the results of the catalytic tests presented in this paper, Ni/CeZrO<sub>2</sub> shows high activity in SRT. If the step of dissociative adsorption of C<sub>7</sub>H<sub>4</sub> molecules to form surface carbon species is fast and the oxidation of those carbon species is slow, the catalyst may suffer deactivation due to carbon accumulation. The excess of H<sub>2</sub>O in the reaction feed helps to suppress carbon species from the catalyst surface and inhibits carbon build-up. However, the application of a high S/C ratio may negatively influence the morphology of the catalyst. Specifically, it may cause the sintering of the Ni particles, leading to the decrease of the catalytically active surface. Moreover, when the catalyst is exposed to elevated temperatures and a high steam concentration, the CeZrO<sub>2</sub> phase can also agglomerate and cover the Ni phase, reducing its accessibility to the reagents. The impact of the S/C ratio on the morphology of Ni/CeZrO<sub>2</sub> was examined by using X-ray diffraction (XRD) and scanning electron microscopy (SEM).

The results of the XRD analyses of Ni/CeZrO<sub>2</sub> before SRT and after tests carried out at S/C = 1 and 4 are presented in Figure 2. The typical reflexes of the CeZrO<sub>2</sub> phase are observed, e.g., at  $2\theta = 28.8, 33.8, 48.5, 58.6^\circ$ , while the small-intensity reflexes of the Ni<sup>0</sup> are detected at  $44.5$  and  $52.6^\circ$ . The mean size of Ni and CeZrO<sub>2</sub> crystallites calculated from the Scherrer equation increases with the S/C ratio applied during the catalytic tests. For the Ni crystallites oriented in the (111) direction, the rise of the mean size from 12.0 nm (fresh catalyst) to 15.0 nm (after tests at S/C = 1) and 20.4 nm (after tests at S/C = 4) was noticed. The mean size of CeZrO<sub>2</sub> crystallites oriented in the (220) direction increased from 8.3 nm to 9.6 and 15.2 nm after tests conducted at S/C = 1 and 4, respectively. Hence, high steam content in the reaction mixture causes the sintering of the support and the active phase, which results in the loss of the catalytically active surface.

The experiments of N<sub>2</sub> sorption (Table 3) revealed that the specific surface area ( $S_{BET}$ ) of the fresh and spent Ni/CeZrO<sub>2</sub> is very similar. Nevertheless, some increase in the mean pore size can be observed for the samples after tests conducted at high steam excess (especially at S/C = 4). As was observed by the XRD, the extended exposition to H<sub>2</sub>O at increased temperatures led to the sintering of the catalyst particles, and during this process some small pores could have experienced coarsening to form bigger ones. Nevertheless, the SEM observations (Figure 3) did not show significant changes in Ni/CeZrO<sub>2</sub> morphology after SRT tests conducted under different S/C ratios.

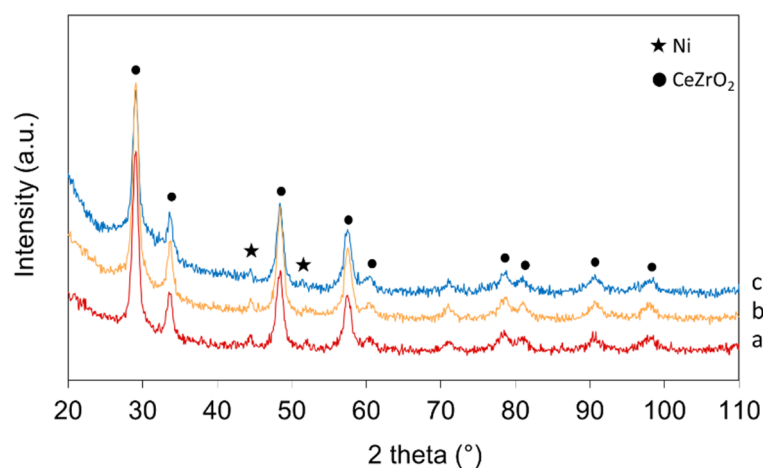


**Figure 2.** The XRD patterns of the Ni/CeZrO<sub>2</sub> catalyst: fresh (a) and spent in SRT at S/C = 1 (b) and S/C = 4 (c).

**Table 3.** The textural properties of Ni/CeZrO<sub>2</sub> before and after catalytic runs of SRT.

Ni/CeZrO <sub>2</sub>	S <sub>BET</sub> (m <sup>2</sup> /g)	d (nm)
before SRT	66	14.91
after SRT at S/C = 1	78	14.12
after SRT at S/C = 2.4	62	15.64
after SRT at S/C = 4	65	19.62

S<sub>BET</sub>—specific surface area calculated using the Brunauer-Emmet-Teller method; d—mean pore size.

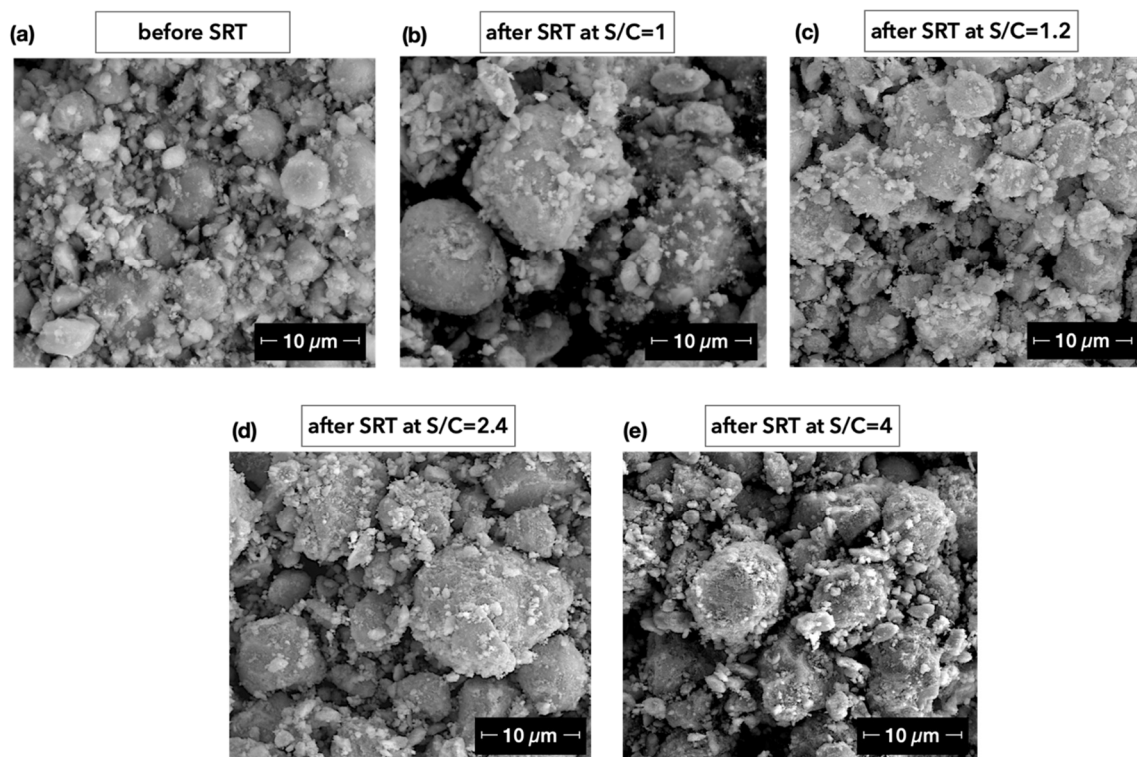


**Figure 3.** SEM images of Ni/CeZrO<sub>2</sub> before reaction (a) and after catalytic tests carried out at S/C = 1 (b), S/C = 1.2 (c), S/C = 2.4 (d) and S/C = 4 (e).

The experiments of N<sub>2</sub> sorption also revealed some minor increases in the catalyst's surface area after SRT was carried out at S/C = 1 (Table 3). It could be related to the

presence of carbon deposits detected by SEM (Figure 4), especially to the filamentous carbons. According to TEM (Figure 5), the structural carbon deposits which have formed on Ni/CeZrO<sub>2</sub> are tubular and curly (Figure 5a). It can be noticed that the rhombohedral nanoparticles of Ni/CeZrO<sub>2</sub> are attached individually or as agglomerates to the walls of CNTs (Figure 5a–c). Concerning the morphology of the obtained structural carbon deposits, one can state that both the bamboo-like carbon nanofibers (CNFs) and the carbon nanotubes (CNTs) may form during SRT carried out at S/C = 1. The outer diameters of the structures pictured in Figure 5b–d range from ca. 20 to 80 nm. The detection of those structures in the Ni/CeZrO<sub>2</sub> sample with TEM was difficult. Firstly, the deposits were located only in some areas of the sample, and secondly, the catalyst was found to be very resistant to carbon deposition, so the concentration of the filamentous carbon species was very low. The structural carbon deposits were not observed in the Ni/CeZrO<sub>2</sub> samples after SRT carried out in the excess of H<sub>2</sub>O (i.e., at S/C = 1.2, 2.4, and 4). According to the TGA, the weight loss of the Ni/CeZrO<sub>2</sub> sample spent in SRT at S/C = 1 (Table 4) was only 5.4%, which corresponds to 0.45 mg of carbon deposited over 1g of catalyst per 1 h of the test run. For example, Zhou et al. [24] reported that the amount of carbon deposited over Pt/Ce<sub>1-x</sub>Zr<sub>x</sub>O<sub>2</sub> was 1.7 mg/g<sub>cat</sub>/h; 3.8 times more than for the Ni/CeZrO<sub>2</sub> reported here. From Table 4, it is evident that even a small increase in S/C, i.e., from 1 to 1.2, considerably enhances the suppression of the carbon species left on the catalyst surface during hydrocarbon dehydrogenation, reducing carbon deposition from 0.45 to 0.26 mg/g<sub>cat</sub>/h. The impressive reduction of carbon accumulation during SRT over Ni/CeZrO<sub>2</sub> can be observed at S/C = 4. Zhu et al. [16], who studied the Ni/Al<sub>2</sub>O<sub>3</sub> catalyst in SRT, also noticed the decrease in coke formation when the S/C increased. According to their work, 0.29, 0.22 and 0.17 g of carbon deposited per 1 g of the catalyst after 5 h time-on-stream at S/C = 1, 2, and 3, respectively. Converted to mg/g<sub>cat</sub>/h, it gives the following values: 58, 44, and 34, which are drastically higher than for the Ni/CeZrO<sub>2</sub> reported here. However, such a comparison is only sketchy. There are few factors that play a role in increased C deposition over Ni/Al<sub>2</sub>O<sub>3</sub> [16] and must be underlined here: (i) the Ni loading, which was 20 wt.%, i.e., twice as high as in the case of Ni/CeZrO<sub>2</sub> (this is very important since Ni is the site for C deposition), (ii) the support, which is not reducible, and unlike CeZrO<sub>2</sub>, does not provide the active oxygen species for suppressing carbon species, and (iii) the contact time as low as  $1.6 \times 10^{-5}$  s (shorter contact times results in increased coke formation;  $t_c$  in the present work is 0.36 s).

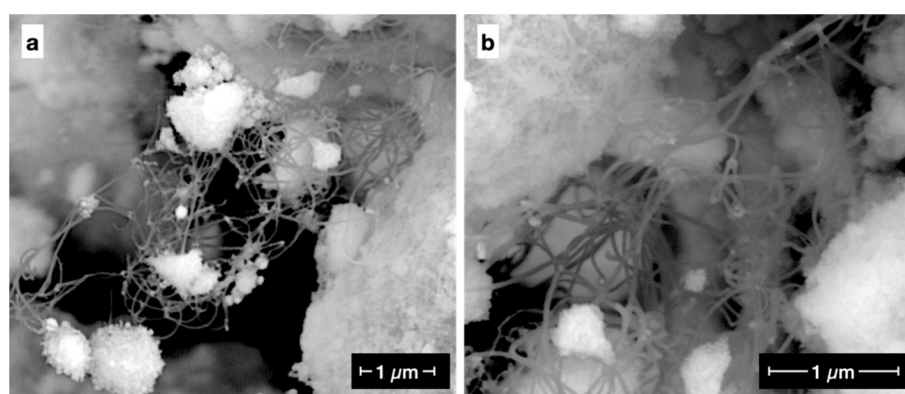


**Figure 4.** SEM images of the Ni/CeZrO<sub>2</sub> catalyst after toluene steam reforming carried out at S/C = 1.

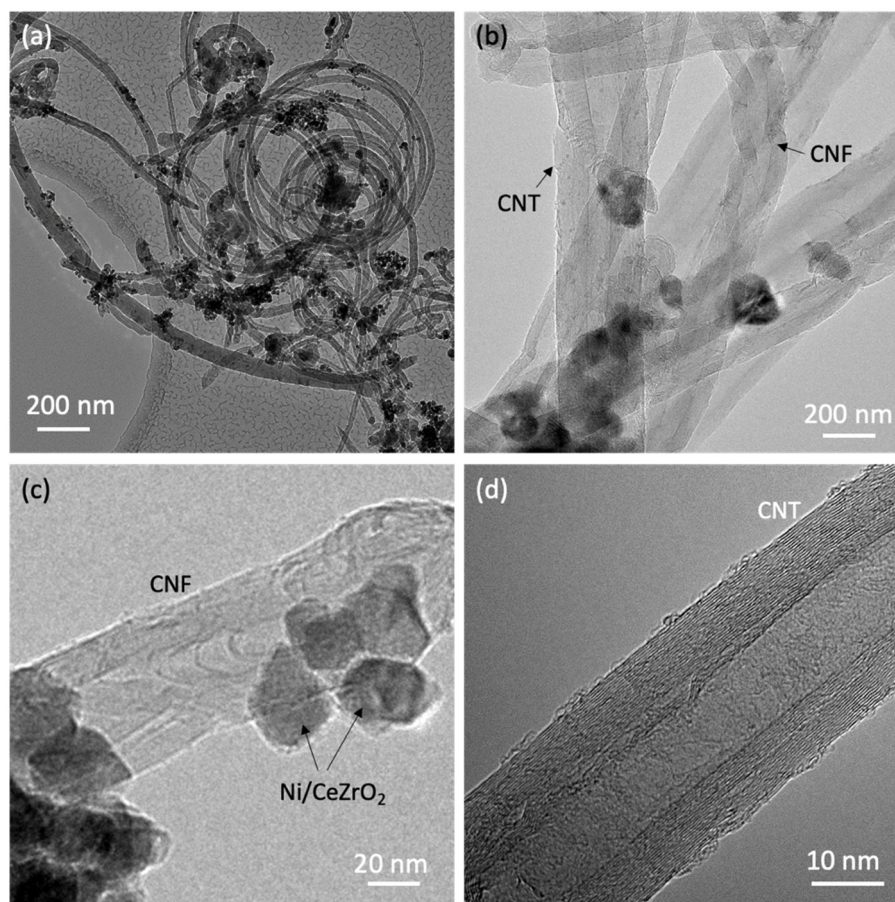


**Figure 5.** TEM images of the carbon deposits formed on the Ni/CeZrO<sub>2</sub> catalyst during toluene steam reforming carried out at S/C = 1.

**Table 4.** The weight loss and carbon deposition rate for the Ni/CeZrO<sub>2</sub> samples after toluene steam reforming carried out at different S/C ratios at temperatures ranging from 420 to 800 °C ( $t_c = 0.36$  s, TOS at each temperature = 24 h).

S/C	Weight Loss (%)	C (mg/g <sub>cat</sub> /h)
1	5.4	0.45
1.2	3.1	0.26
2.4	1.6	0.13
4	0.6	0.05

Based on the obtained results, the reaction pathways for the formation of filamentous carbon during SRT over Ni/CeZrO<sub>2</sub> can be proposed (Figure 6).

The toluene molecule adsorbs on the Ni active site, which leads to its demethylation. The first route of filamentous carbon formation (I) assumes the formation of a biphenyl from two adsorbed phenyl groups. The combination of a few biphenyls leads first to the graphene layer, which can stack and roll up to form CNT [41]. The biphenyl formation via dissociation of the C-I bond in iodobenzene adsorbed over Cu (111) was studied by Xi and Bent [45]. The authors reported that phenyl groups adsorb on Cu (111) with their  $\pi$ -rings approximately parallel to the surface. These phenyl groups were found to be thermally stable to above 300 K, while above that temperature they can couple to form a biphenyl. The decomposition of hydrocarbon can lead to graphite layers and to the formation of CNFs [46,47]. The radical mechanism of the formation of bipyridyl molecule catalyzed by Ni (111) using a pyridine precursor was studied by the DFT (density functional theory) calculations by Feng et al. [48]. In that work, the bipyridyl was assumed as the initial

process of the growth of N-doped graphene. In the second route (II), CNTs or CNFs are obtained from methane decomposition. The molecules of  $\text{CH}_4$  are released to the gas phase after the hydrogenation of the methyl groups adsorbed on the metal active site after toluene demethylation. The filamentous carbon can be also formed from CO (route III), which is a product of the steam reforming reaction. According to [49], the potential of aromatic molecules towards carbon formation is reported to be several times higher than CO or methane.

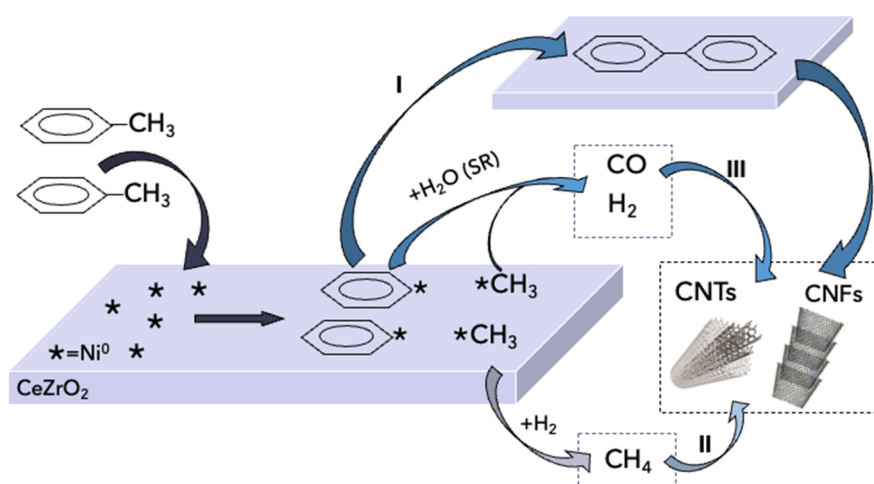


**Figure 6.** The scheme of CNTs and CNFs formation on the Ni/CeZrO<sub>2</sub> surface during the steam reforming of toluene. Possible routes: I—via biphenyl, II—from CH<sub>4</sub> dehydrogenation, and III—from CO disproportionation.

### 2.3. The Influence of Contact Time

The influence of contact time ( $t_c$ ) on toluene conversion and hydrogen yield during the steam reforming reaction carried out at different S/C ratios is presented in Figure 7. For all experiments, the increase in contact time increases toluene conversion and hydrogen yield. From the presented graph, the impact of  $t_c$  is more pronounced at lower temperatures. As the temperature increases (for each S/C ratio), the dissimilarities in  $\text{C}_7\text{H}_8$  conversions and  $\text{H}_2$  yields for different  $t_c$  values are less significant. Toluene steam reforming, as an endothermic reaction, favors high temperatures. At elevated temperatures, the rate of reaction is high; hence, the impact of parameters such as S/C or  $t_c$  on toluene conversion is minor. At lower temperatures, the rate of SRT decreases, thus the effect of S/C and  $t_c$  is more pronounced. From the collected data, one can say that the performance of Ni/CeZrO<sub>2</sub> at lower temperatures (420–600 °C) can be significantly improved by increasing the contact time, while at higher temperatures, the impact of  $t_c$  is not that profound. For all experiments, toluene conversion increases with reaction temperature. The increase in hydrogen yield with temperature is observed only for S/C = 1 and 1.2, while for the experiments carried out at higher steam excess (at S/C = 2.4 and 4), the  $\text{H}_2$  yield decreases above 500 °C owing to the thermodynamic limitations of the WGS reaction (Equation (3)).

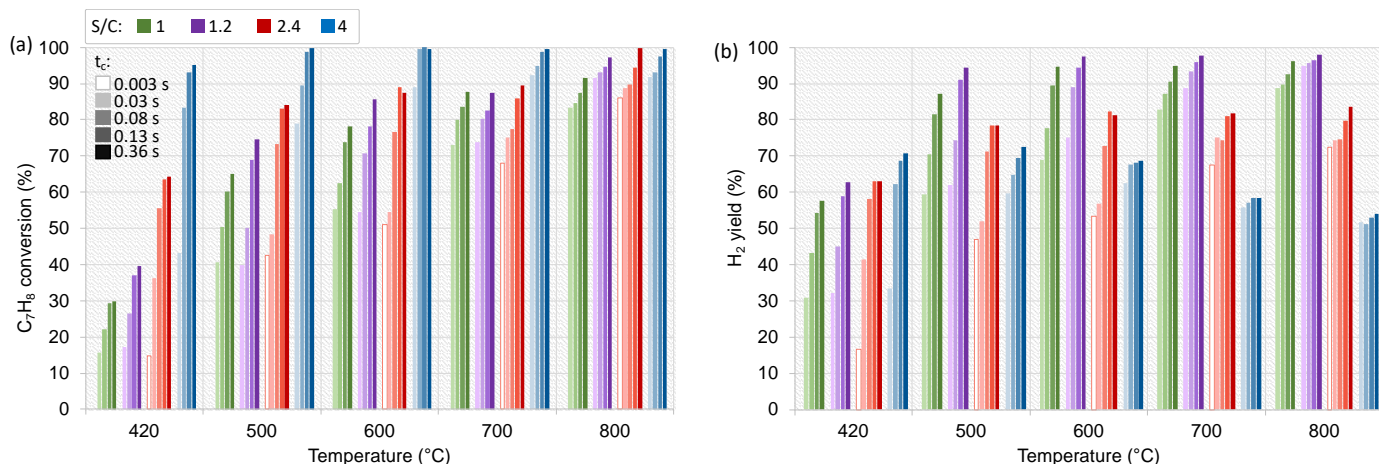
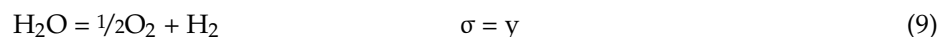
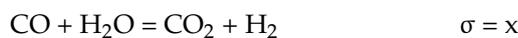
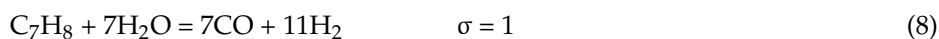


**Figure 7.** The influence of contact time ( $t_c$ ) on  $C_7H_8$  conversion (a) and  $H_2$  yield (b) vs. temperature during the catalytic runs of SRT carried out in stationary conditions with the S/C ratios of 1 (green), 1.2 (purple), 2.4 (red), and 4 (blue). The darker the shade of the bar, the higher the  $t_c$  value.

The calculation of the  $H_2/CO$  and  $H_2/(CO + CO_2)$  ratios can give more insight into the phenomena occurring during the SRT reaction over  $Ni/CeZrO_2$ , such as the “overproduction” of hydrogen. The steam reforming reaction, especially when conducted under steam excess, is accompanied by a WGS reaction. Moreover, the presence of reduced cerium species in the  $CeZrO_2$  allows for  $H_2O$  dissociation to  $H_2$  and lattice oxygen. The  $H_2/CO$  will be more suitable to describe the SRT conducted at stoichiometric steam content ( $S/C = 1$ ), while the  $H_2/(CO + CO_2)$  is the proper one to explain the WGS-accompanied SRT because it also considers the  $CO$  which was produced in the SR reaction but was further converted into  $CO_2$  in the WGS reaction. An overall reaction of toluene conversion concerning the participation of three steps, i.e., SRT (Equation (8)), WGS (Equation (3)) and  $H_2O$  dissociation (Equation (9)), may be written as Equation (10). The  $\sigma$  is the stoichiometric number of the step. The  $H_2/CO$  and  $H_2/(CO + CO_2)$  ratios are expressed by Equations (11) and (12). By knowing the experimental values of both ratios (presented in Figure 8), one can calculate the stoichiometric numbers for the WGS step ( $x$ ) and the  $H_2O$  dissociation step ( $y$ ).



$$H_2/CO = (11 + x + y)/(7 - x) \quad (11)$$

$$H_2/(CO + CO_2) = (11 + x + y)/7 \quad (12)$$

For the SRT reaction taking place alone, “ $x$ ” and “ $y$ ” value zero. In such a case, the  $H_2/(CO + CO_2)$  and  $H_2/CO$  are equal (because  $CO_2$  is not produced) and amount to 1.57. If  $H_2/CO$  is above that value, it indicates the occurrence of the parallel reactions producing  $H_2$  (Equations (3) and (9)) and is typical for the ceria-zirconia supported metal catalyst. Figure 8 shows the  $H_2/CO$  and  $H_2/(CO + CO_2)$  ratios as a function of temperature during the SRT catalytic test carried out under changing  $t_c$  and at different steam excess.

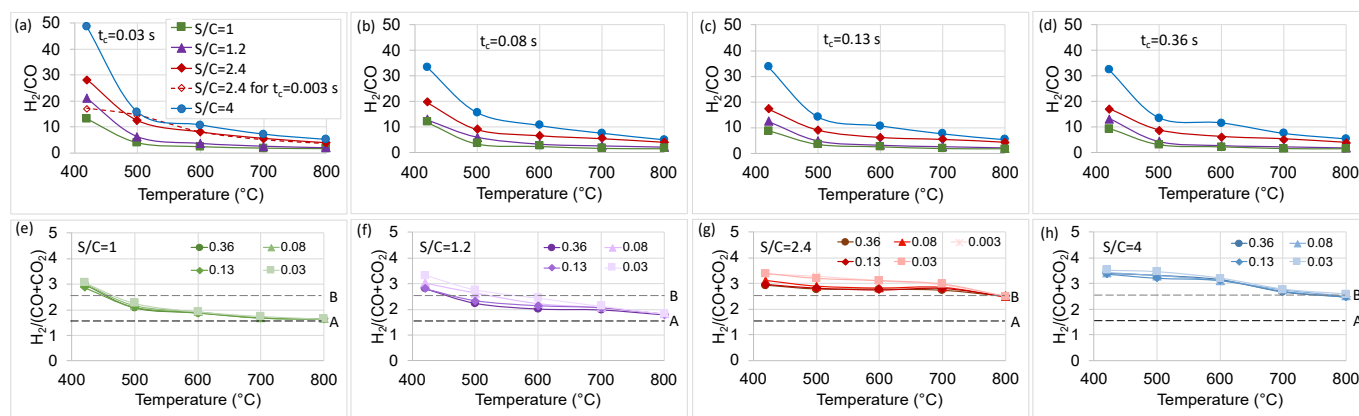
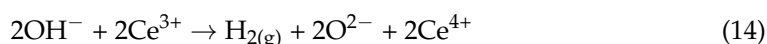
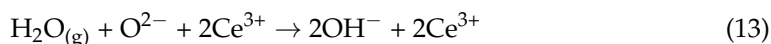


**Figure 8.** The  $H_2/CO$  (a–d) and  $H_2/(CO + CO_2)$  ratios (e–h) during toluene steam reforming carried out at different S/C ratios and various contact times. The  $H_2/(CO + CO_2)$  value of 1.57 (for  $x = 0$ ,  $y = 0$ ) is indicated with line A, and of 2.57 (for  $x = 7$ ,  $y = 0$ ) with line B.

For all S/C ratios and contact times, the  $H_2/CO$  (Figure 8a–c) exceeds 1.57, indicating the occurrence of said parallel reactions. The highest production of hydrogen out of the steam reforming catalytic cycle is observed for higher S/C ratios and at lower temperatures (especially at 420 °C, and to a lesser extent at 500 °C). This is explained by the fact that at high steam concentrations, the WGS equilibrium is shifted towards  $H_2$  production, not to mention that this reaction favors low temperatures. The  $H_2/(CO + CO_2)$  ratios (Figure 8d–h) also show an overproduction of hydrogen because their values exceed 1.57 (marked with dotted line “A”).

It can be observed that the contact time has no effect or a minor effect on the  $H_2/(CO + CO_2)$  ratios. Some influence of contact time is noticed at lower temperatures and for lower  $t_c$  values. The increase in S/C ratio increases  $H_2/(CO + CO_2)$ , owing to increased participation of WGS reaction. If the stoichiometric number of the WGS reaction “ $x$ ” (Equation (3)) reaches its maximal value of 7 (because one catalytic cycle of SRT gives 7 moles of CO, and each mole of CO can be converted into 1 mole of  $CO_2$  within one catalytic cycle of WGS), the  $H_2/(CO + CO_2)$  is equal to 2.57, and that is indicated with line “B”. It can be seen from the graphs in Figure 8g and h that the application of high steam excess (S/C = 2.4 and 4) results in significant overproduction of  $H_2$  in the whole range of applied temperatures.

One must remember that except for the SRT and WGS, another reaction which produces hydrogen during toluene steam reforming over the studied Ni/CeZrO<sub>2</sub> catalyst is  $H_2O$  dissociation (Equation (9)). The adsorptive dissociation of steam occurs on oxygen vacancies and surface oxygen ( $O^{2-}$ ) of ceria-zirconia and produces  $H_2$  and  $Ce^{4+}$  via formation of the surface hydroxyl ( $OH^-$ ) as described by Equations (13) and (14) [50]. These reactions are the elementary steps occurring within the catalytic cycles of SRT and WGS reactions; however, owing to the nature of CeZrO<sub>2</sub> support, they can also take place beyond those cycles, increasing the overall  $H_2$  production.



The formation of oxygen vacancies in pure ceria starts from 350 °C [51], thus allowing the formation of oxygen vacancies on which  $H_2O$  can dissociate—also beyond the catalytic cycles of the SR and WGS reactions. It is also widely known that the formation of oxygen vacancies is facilitated when ceria is doped with zirconium, because due to the smaller ionic radius of the Zr compared to Ce, the mobility of the surface oxygen is increased.

The surface hydroxyls that form during  $H_2O$  dissociative adsorption are thermally stable up to 130–330 °C and may produce either  $H_2$  or  $H_2O$  [52,53]. The DFT calculations

performed by Hansen and Wolverton [50] revealed that H<sub>2</sub>O adsorbed near the surface vacancy easily dissociates to OH<sup>−</sup>. This step is highly exothermic. Whereas the decomposition of hydroxyls to H<sub>2</sub> requires the breakage of the O-H bond and is endothermic. On a fully hydroxylated ceria, the OH<sup>−</sup> species can decompose to H<sub>2</sub> at high temperatures. Also, according to Henderson [54], the rate of H<sub>2</sub> desorption from the hydroxylated surface of ceria increases with temperature. Carrasco et al. [55] studied Ni/CeO<sub>2</sub> (111) in H<sub>2</sub>O dissociation and found that Ni<sup>2+</sup> sites support the dissociation of the O-H bond. Those Ni<sup>2+</sup> sites are generated by the strong metal-support interaction or by the formation of Ce<sub>1−x</sub>Ni<sub>x</sub>O<sub>2−y</sub> solid solutions. On the contrary, the Ni atoms which form clusters and are not in an intimate contact with ceria show low activity in H<sub>2</sub>O dissociation (which is comparable to the performance of unsupported Ni).

The contribution of H<sub>2</sub> (x) produced in SRT, WGS, and H<sub>2</sub>O dissociation over the Ni/CeZrO<sub>2</sub> catalyst in the product gas from toluene steam reforming was calculated using Equations (15)–(17) and is presented in Figure 9.

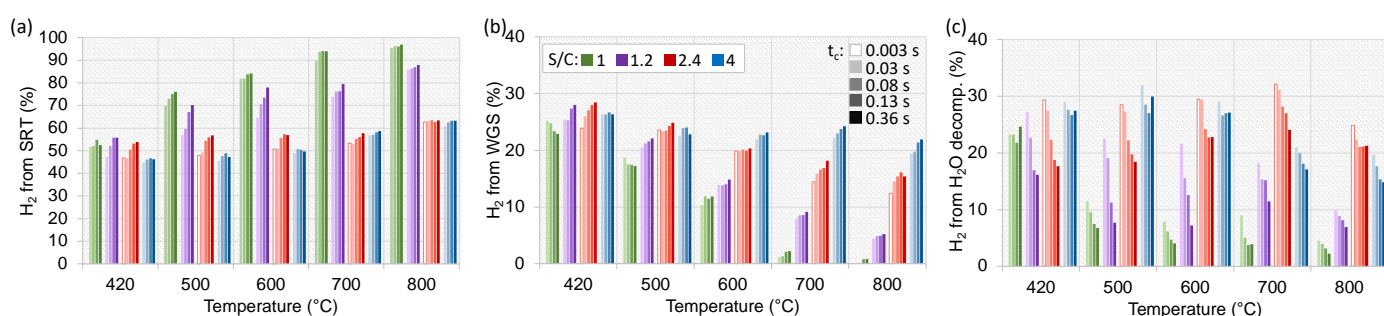


**Figure 9.** The contribution of H<sub>2</sub> produced in the SRT reaction (a), the WGS reaction (b) and the H<sub>2</sub>O decomposition reaction (c) during the catalytic tests of toluene steam reforming carried out at S/C = 1 (green), 1.2 (purple), 2.4 (red), and 4 (blue), with contact time ( $t_c$ ) varying from 0.003 to 0.36 s (the darker the shade of the bar the higher the  $t_c$  value).

$$x_{H_2 \text{ SRT}} = \frac{11 \cdot ([CO]_{(out)} + [CO_2]_{(out)})}{7[H_2]_{(out)}} \cdot 100 [\%] \quad (15)$$

$$x_{H_2 \text{ WGS}} = \frac{[CO_2]_{(out)}}{[H_2]_{(out)}} \cdot 100 [\%] \quad (16)$$

$$x_{H_2 \text{ dissociation}} = 100 - x_{H_2 \text{ SRT}} - x_{H_2 \text{ WGS}} \quad (17)$$

As is displayed in Figure 9a, the contribution of the H<sub>2</sub> produced in the SRT reaction increases with temperature and is the highest at S/C = 1. Moreover, it decreases with increasing steam excess owing to the growing participation of WGS and H<sub>2</sub>O dissociation (Figure 9b,c). As is presented in Figure 10, the stoichiometric numbers of both reactions, i.e., “x” for WGS and “y” for H<sub>2</sub>O dissociation, increase with raising the S/C ratio because more H<sub>2</sub>O is introduced to the reaction feed. In addition, “x” and “y” decrease with temperature owing to the reactions’ thermodynamics. Based on the collected results, one can state that the impact of  $t_c$  on the contribution of both reactions occurring in parallel to SRT is minor, especially at higher temperatures. Nevertheless, to resolve this issue, more sets of catalytic runs should be conducted under varying S/C and  $t_c$ .

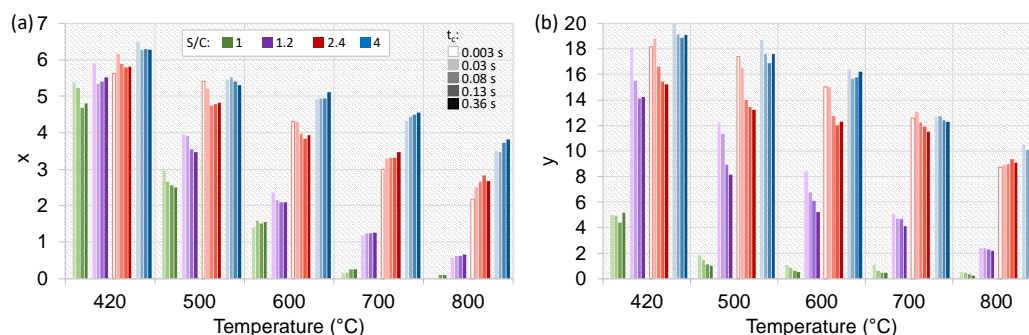


**Figure 10.** The number of catalytic cycles of the WGS (a) and H<sub>2</sub>O dissociation (b) reactions during the catalytic tests of toluene steam reforming carried out at S/C = 1 (green), 1.2 (purple), 2.4 (red), and 4 (blue), and contact times ( $t_c$ ) varying from 0.003 to 0.36 s (the shade of the bar darkens when the  $t_c$  value increases).

Table 5 shows the carbon formation over Ni/CeZrO<sub>2</sub> catalyst during catalytic tests of toluene steam reforming carried out under S/C = 2.4 at different contact times. The highest carbon deposition determined by TGA is observed for the lowest contact time, 0.003 s, and it decreases with increasing  $t_c$ . Hence, the application of higher contact times results in a higher conversion of toluene and H<sub>2</sub> yield (Figure 7) and decreased carbon formation.

**Table 5.** The weight loss of Ni/CeZrO<sub>2</sub> samples and the rate of carbon deposition after toluene steam reforming carried out at S/C = 2.4 and different contact times ( $t_c$ ) at temperatures ranging from 420 to 800 °C (TOS at each temperature = 24 h).

$t_c$ (s)	Weight Loss (%)	C (mg/g <sub>cat</sub> /h)
0.003	6.8	0.57
0.03	3	0.25
0.08	1.8	0.15
0.13	1.7	0.14
0.36	1.6	0.13

#### 2.4. Stability Tests

The stability tests of toluene steam reforming were conducted at 600, 700, and 800 °C. Those experiments were carried out at S/C = 2.4 because such an excess of steam in the reaction feed ensures a good resistance of the catalyst both to carbon deposition and to sintering. Figure 11 shows that toluene conversions after 120 h of test-run at 600, 700, and 800 °C reach 75, 90, and 95%, respectively, whereas hydrogen yields are 70, 77, and 80%. The highest production of CO<sub>2</sub> is observed at 600 °C (42%) owing to the most important participation of the WGS reaction. On the contrary, at the temperatures as high as 800 °C, the CO<sub>2</sub> yield is only 28%. The obtained results prove that Ni/CeZrO<sub>2</sub> is very active and a stable catalyst for toluene steam reforming, even at 600 °C.

The TGA performed for spent catalysts revealed the weight loss (assigned to oxidation of carbon deposits) equal to 3.8 wt.% (at 600 °C), 1.9 wt.% (at 700 °C), and 1.3 wt.% (at 800 °C) (Table 6). Hence, the amount of deposited carbon was low, especially when the SRT reaction was carried out at elevated temperatures. No change in the textural properties of Ni/CeZrO<sub>2</sub> was noticed. The S<sub>BET</sub> for the samples spent at 600, 700, and 800 °C were 64, 66, and 67 m<sup>2</sup>/g, respectively, which indicates that the catalyst is characterized by a very good stability.

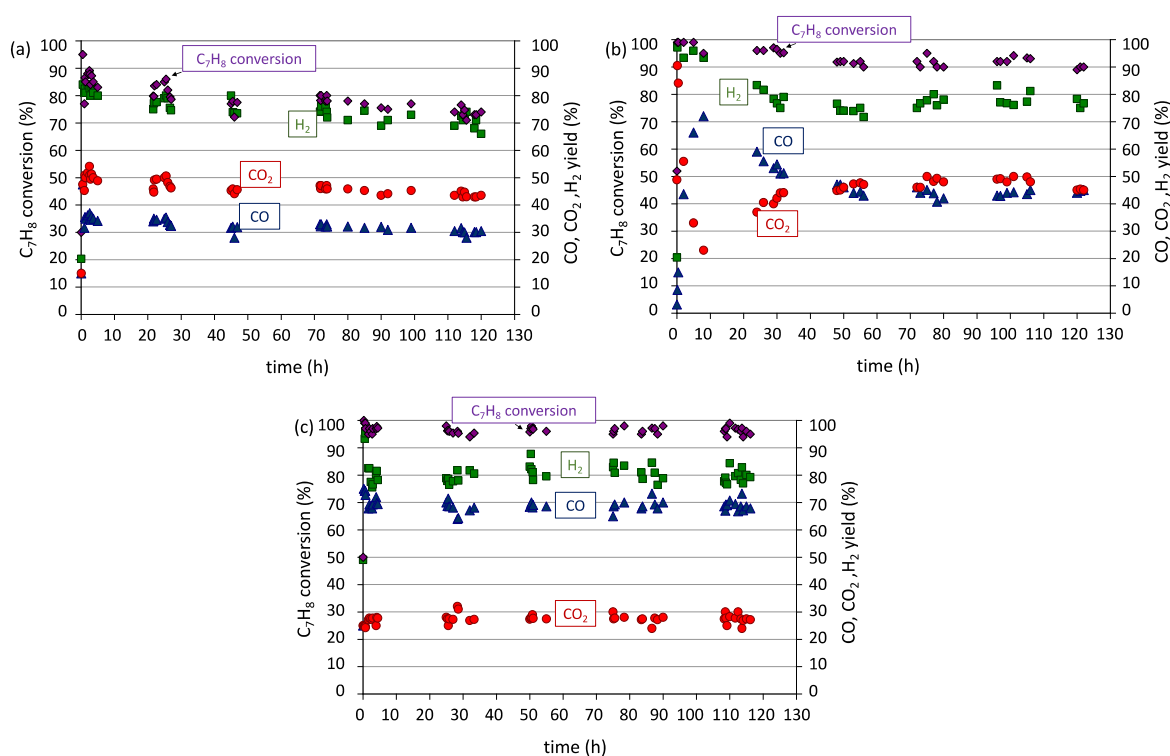


**Figure 11.** The toluene conversion and products' (CO, CO<sub>2</sub>, H<sub>2</sub>) yields during stability tests of toluene steam reforming over Ni/CeZrO<sub>2</sub> carried out at S/C = 2.4 and t<sub>c</sub> = 0.36 s at 600 °C (a), 700 °C (b), and 800 °C (c).

**Table 6.** The weight loss of Ni/CeZrO<sub>2</sub> samples and the rate of carbon deposition after stability tests of toluene steam reforming carried out S/C = 2.4 and t<sub>c</sub> = 0.36 s.

T (°C)	Weight Loss (%)	C (mg/g <sub>cat</sub> /h)
600	3.8	0.32
700	1.9	0.16
800	1.3	0.11

### 3. Materials and Methods

**Catalyst synthesis.** The preparation and characterization of a ceria-zirconia-supported nickel catalyst were presented in [5]. The nominal loading of Ni over CeZrO<sub>2</sub> was 10 wt.%.

**Catalytic tests.** The Ni/CeZrO<sub>2</sub> catalyst was first reduced in situ at 700 °C for 1.5 h in 5 vol.% of H<sub>2</sub> in Ar (flowing rate of 100 mL/min) and then purged with Ar at 800 °C for 1 h (flowing rate of 100 mL/min). The catalyst pre-reduction was made to eliminate the step of the total oxidation of toluene to CO<sub>2</sub> and H<sub>2</sub>O, which typically occurs on the metal oxide and leads to a zero-valent metal, but also takes place over the Ce<sup>4+</sup>, reducing it to Ce<sup>3+</sup>. After purging the catalyst bed with Ar at 800 °C, the reaction mixture composed of toluene (0.25 vol.%, POCH, Gliwice, Poland), water steam (varying concentrations), and Ar as a balance was introduced. After 4 h (or 24 h) of a test run at 800 °C, the temperature was first decreased to 700 °C, and next to 600, 500, and finally to 420 °C, and kept for 4 h (or 24 h) at each T. Tests were carried out at S/C = 1, 1.2, 2.4, and 4. For each S/C ratio, four different contact times were applied: 0.03, 0.08, 0.13, and 0.36 s. Additionally, for S/C = 2.4, a catalytic run at t<sub>c</sub> = 0.003 s was carried out. The stability tests of toluene steam reforming over Ni/CeZrO<sub>2</sub> were carried out at 600, 700, and 800 °C for 120 h at each temperature. During those tests, the applied S/C was 2.4 and t<sub>c</sub> was 0.36 s. Each stability test was conducted using the new pre-reduced catalyst sample.

The products of toluene SR were determined by gas chromatograph with a thermal conductivity detector (Ai Scientific, Cambridge, England). Toluene conversion to CO and

CO<sub>2</sub> was calculated using Equation (18). The yields of gaseous products, i.e., H<sub>2</sub>, CO, and CO<sub>2</sub>, were calculated using Equations (20), (22) and (23).

$$C_7H_8 \text{ conversion} = \frac{[C_7H_8]_{(SR)} \cdot 100}{[C_7H_8]_{(in)}} (\%) \quad (18)$$

$$[C_7H_8]_{(SR)} = \frac{[CO]_{(out)} + [CO_2]_{(out)}}{7} \left( \text{mol/dm}^3 \right) \quad (19)$$

$$H_2 \text{ yield} = \frac{[H_2]_{(out)}}{[H_2]_{(in)}} \cdot 100 (\%) \quad (20)$$

$$[H_2]_{(in)} = 4 \cdot [C_7H_8]_{(in)} + [H_2O]_{(in)} \left( \text{mol/dm}^3 \right) \quad (21)$$

$$CO \text{ yield} = \frac{[CO]_{(out)}}{7 \cdot [C_7H_8]_{(in)}} \cdot 100 (\%) \quad (22)$$

$$CO_2 \text{ yield} = \frac{[CO_2]_{(out)}}{7 \cdot [C_7H_8]_{(in)}} \cdot 100 (\%) \quad (23)$$

where:

$[C_7H_8]_{SR}$ —the concentration of C<sub>7</sub>H<sub>8</sub> converted in SR reaction to CO and CO<sub>2</sub>;

$[C_7H_8]_{(in)}$ ,  $[H_2O]_{(in)}$ ,  $[H_2]_{(in)}$ —the concentrations of C<sub>7</sub>H<sub>8</sub>, H<sub>2</sub>O, and H<sub>2</sub> in the feed;

$[H_2]_{(out)}$ ,  $[CO_2]_{(out)}$ ,  $[CO]_{(out)}$ —the concentrations of H<sub>2</sub>, CO<sub>2</sub>, and CO at the reactor's outlet.

In addition, to determine the amounts of unreacted toluene and reaction by-products, the gas was analyzed by GC-MS (Perkin Elmer, Waltham, MA, USA). These analyses were performed during the catalytic runs of toluene SR at temperatures ranging from 500 to 900 °C at S/C = 2.4 and t<sub>c</sub> = 0.36 s.

*Catalyst's characterization.* The X-ray diffraction (XRD) measurements were performed with a TUR-M62 diffractometer (Carl Zeiss, Jena, Germany) with a copper anticathode (λ = 1.54 Å), 34 kV voltage, and 25 mA current. The XRD patterns were acquired for 2θ angles ranging from 20 to 100°, with 0.03° steps. The crystallographic structures of the samples and the Miller indices (hkl) of the diffraction lines were determined using bibliographic data published by the Joint Committee on Powder Diffraction Standards (JCPDS cards No. 01-078-0694 and 04-0850 for CeZrO<sub>2</sub> and Ni, respectively). The mean crystallite sizes of CeZrO<sub>2</sub> and Ni were determined using the Scherrer equation (Equation (24)).

$$D_{(hkl)} = \frac{K\lambda}{B \cdot \cos\Theta_{(hkl)}} \text{ (nm)} \quad (24)$$

where:  $D_{(hkl)}$ —the size of crystallite in (hkl) direction;  $K$ —Scherrer constant (0.9);  $\lambda$ —the X-ray wavelength (0.1548 nm);  $B$ —the full width at half max of diffraction peak (rad);  $\Theta_{(hkl)}$ —the diffraction angle.

Microscopic studies were performed using a high-resolution scanning electron microscope Quanta 250 FEG (FEI Company, Hillsboro, OR, USA) and high resolution transmission electron microscope JEM 2011 (JEOL, Japan, Tokyo) associated with a top entry device and operating at 200 kV.

The N<sub>2</sub> sorption was performed using the Sorptomatic 1800 (Carlo Erba, Egelsbach, Germany) at 77 K. Prior to analyses, the samples were outgassed at 150 °C for 12 h. The average pore size and pore volume were calculated using the Barrett–Joyner–Halenda (BJH) method.

The thermogravimetric analyses (TGA) were conducted by using a derivatograph Q-1500 (TA Instruments, Budapest, Hungary). The experiments were carried out under ambient pressure and air flowing with a rate of 100 mL/min. The experimental temperature ranged from about 25 °C to 900 °C with a heating rate of 10 °C /min.

#### 4. Conclusions

The Ni/CeZrO<sub>2</sub> catalyst was tested in toluene steam reforming under varying steam excess and contact times. The catalyst exhibited very high toluene conversion and H<sub>2</sub> yields, very good stability, and a high resistance to carbon deposition.

It was confirmed that the performance of Ni/CeZrO<sub>2</sub> was improved when the S/C ratio and contact time increased. The impact of both parameters was more important at lower temperatures. For example, it was observed that the activity of Ni/CeZrO<sub>2</sub> at lower temperatures (420–600 °C) can be significantly improved by increasing the contact time.

Conducting the steam reforming reaction under H<sub>2</sub>O excess prevents the catalyst deactivation caused by carbon deposition. Firstly, H<sub>2</sub>O is a source of the active oxygen for the oxidation of carbon species on the catalyst surface. Secondly, steam excess reduces toluene dealkylation to benzene, which may accumulate on the catalyst surface, forming structural carbon deposits. In this work, benzene formation was negligible or did not take place when the S/C was 2.4 and 4. Formation of the filamentous carbons (CNTs and CNFs) during toluene steam reforming was observed only when S/C was 1. Even under such conditions, the formation of carbon deposits was low thanks to the properties of ceria-zirconia support, which provides the active sites for H<sub>2</sub>O dissociation. This reaction is an elementary reaction within the steam reforming and WGS catalytic cycles. However, as was confirmed in this study, H<sub>2</sub>O dissociation can also occur beyond those cycles, providing more active oxygen to the catalyst and enriching the product gas in H<sub>2</sub>.

**Funding:** This work was financed by a statutory activity subsidy from the Polish Ministry of Science and Higher Education for the Faculty of Chemistry of Wrocław University of Science and Technology. Studies of carbon deposits were financed by the Ministry of Science and Higher Education, project Iuventus Plus, IP2011030871.

**Data Availability Statement:** The data presented in this study are available on request from the corresponding author.

**Acknowledgments:** The Ministry of Science and Higher Education is acknowledged for financing the studies on carbon deposits (Iuventus Plus program, project No. IP2011030871).

**Conflicts of Interest:** The author declares no conflict of interest.

#### References

1. Anis, S.; Zainal, Z.A. Tar reduction in biomass producer gas via mechanical, catalytic and thermal methods: A review. *Renew. Sust. Energy Rev.* **2011**, *15*, 2355–2377. [[CrossRef](#)]
2. Devi, L.; Ptasiński, K.J.; Janssen, F.J.J.G. Pretreated olivine as tar removal catalyst for biomass gasifiers: Investigation using naphthalene as model biomass tar. *Fuel Process. Technol.* **2005**, *86*, 707–730. [[CrossRef](#)]
3. Nair, S.A.; Yan, K.; Pemen, A.J.M.; van Heesch, E.J.M.; Ptasiński, K.J.; Drinkenburg, A.A.H. Tar Removal from Biomass-Derived Fuel Gas by Pulsed Corona Discharges. A Chemical Kinetic Study. *Ind. Eng. Chem. Res.* **2004**, *43*, 1649–1658. [[CrossRef](#)]
4. Jess, A. Mechanisms and kinetics of thermal reactions of aromatic hydrocarbons from pyrolysis of solid fuels. *Fuel* **1996**, *75*, 1441–1448. [[CrossRef](#)]
5. Łamacz, A.; Krztoń, A.; Musi, A.; Da Costa, P. Reforming of Model Gasification Tar Compounds. *Catal. Lett.* **2008**, *128*, 40–48. [[CrossRef](#)]
6. Łamacz, A.; Krztoń, A.; Djéga-Mariadassou, G. Steam reforming of model gasification tars compounds on nickel based ceria-zirconia catalysts. *Catal. Today* **2011**, *176*, 347–351. [[CrossRef](#)]
7. Laosiripojana, N.; Assabumrungrat, S. Catalytic steam reforming of ethanol over high surface area CeO<sub>2</sub>: The role of CeO<sub>2</sub> as an internal pre-reforming catalyst. *Appl. Catal. B Environ.* **2006**, *66*, 29–39. [[CrossRef](#)]
8. Huang, T.; Huang, M. Effect of Ni content on hydrogen production via steam reforming of methane over Ni/GDC catalysts. *Chem. Eng. J.* **2008**, *145*, 149–153. [[CrossRef](#)]
9. Machocki, A.; Denis, A.; Grzegorzczak, W.; Gac, W. Nano- and micro-powder of zirconia and ceria-supported cobalt catalysts for the steam reforming of bio-ethanol. *Appl. Surf. Sci.* **2010**, *256*, 5551–5558. [[CrossRef](#)]
10. Laosiripojana, N.; Sangtongkitcharoen, W.; Assabumrungrat, S. Catalytic steam reforming of ethane and propane over CeO<sub>2</sub>-doped Ni/Al<sub>2</sub>O<sub>3</sub> at SOFC temperature: Improvement of resistance toward carbon formation by the redox property of doping CeO<sub>2</sub>. *Fuel* **2006**, *85*, 323–332. [[CrossRef](#)]

11. Laosiripojana, N.; Assabumrungrat, S. Catalytic steam reforming of dimethyl ether (DME) over high surface area Ce–ZrO<sub>2</sub> at SOFC temperature: The possible use of DME in indirect internal reforming operation (IIR-SOFC). *Appl. Catal. A Gen.* **2007**, *320*, 105–113. [[CrossRef](#)]
12. Borowiecki, T.; Denis, A.; Gac, W.; Dziembaj, R.; Piwowarska, Z.; Drozdek, M. Oxidation–reduction of Ni/Al<sub>2</sub>O<sub>3</sub> steam reforming catalysts promoted with Mo. *Appl. Catal. A Gen.* **2004**, *274*, 259–267. [[CrossRef](#)]
13. Wang, Y.; Chin, Y.H.; Rozmiarek, R.T.; Johnson, B.R.; Gao, Y.; Watson, J.; Tonkovich, A.Y.L.; Vander Wiel, D.P. Highly active and stable Rh/MgOAl<sub>2</sub>O<sub>3</sub> catalysts for methane steam reforming. *Catal. Today* **2004**, *98*, 575–581. [[CrossRef](#)]
14. Wu, C.; Liu, R. Carbon deposition behavior in steam reforming of bio-oil model compound for hydrogen production. *Int. J. Hydrog. Energy* **2010**, *35*, 7386–7398. [[CrossRef](#)]
15. Kim, H.-W.; Kang, K.-M.; Kwak, H.-Y.; Kim, J.H. Preparation of supported Ni catalysts on various metal oxides with core/shell structures and their tests for the steam reforming of methane. *Chem. Eng. J.* **2011**, *168*, 775–783. [[CrossRef](#)]
16. Zhu, H.L.; Pastor-Pérez, L.; Millan, M. Catalytic Steam Reforming of Toluene: Understanding the Influence of the Main Reaction Parameters over a Reference Catalyst. *Energies* **2020**, *13*, 813. [[CrossRef](#)]
17. Gołębowski, A.; Stołeczki, K.; Prokop, U.; Kuśmierowska, A.; Borowiecki, T.; Denis, A.; Sikorska, C. Influence of potassium on the properties of steam reforming catalysts. *React. Kinet. Catal. Lett.* **2004**, *82*, 179–189. [[CrossRef](#)]
18. Borowiecki, T.; Giecko, G.; Panczyk, M. Effects of small MoO<sub>3</sub> additions on the properties of nickel catalysts for the steam reforming of hydrocarbons: II. Ni–Mo/Al<sub>2</sub>O<sub>3</sub> catalysts in reforming, hydrogenolysis and cracking of *n*-butane. *Appl. Catal. A Gen.* **2002**, *230*, 85–97. [[CrossRef](#)]
19. Borowiecki, T.; Gac, W.; Denis, A. Effects of small MoO<sub>3</sub> additions on the properties of nickel catalysts for the steam reforming of hydrocarbons: III. Reduction of Ni–Mo/Al<sub>2</sub>O<sub>3</sub> catalysts. *Appl. Catal. A Gen.* **2004**, *270*, 27–36. [[CrossRef](#)]
20. Fornasiero, P.; Balducci, G.; Di Monte, R.; Kašpar, J.; Sergo, V.; Gubitosa, G.; Ferrero, A.; Graziani, M. Modification of the Redox Behaviour of CeO<sub>2</sub> Induced by Structural Doping with ZrO<sub>2</sub>. *J. Catal.* **1996**, *164*, 173–183. [[CrossRef](#)]
21. Zhuang, Q.; Qin, Y.; Chang, L. Promoting effect of cerium oxide in supported nickel catalyst for hydrocarbon steam-reforming. *Appl. Catal.* **1991**, *70*, 1–8. [[CrossRef](#)]
22. Laosiripojana, N.; Assabumrungrat, S. Methane steam reforming over Ni/Ce–ZrO<sub>2</sub> catalyst: Influences of Ce–ZrO<sub>2</sub> support on reactivity, resistance toward carbon formation, and intrinsic reaction kinetics. *Appl. Catal. A Gen.* **2005**, *290*, 200–211. [[CrossRef](#)]
23. Tao, J.; Zhao, L.; Dong, C.; Lu, Q.; Du, X.; Dahlquist, E. Catalytic Steam Reforming of Toluene as a Model Compound of Biomass Gasification Tar Using Ni–CeO<sub>2</sub>/SBA-15 Catalysts. *Energies* **2013**, *6*, 3284–3296. [[CrossRef](#)]
24. Zhou, S.; Chen, Z.; Gong, H.; Wang, X.; Zhu, T.; Zhou, Y. Low-temperature catalytic steam reforming of toluene as a biomass tar model compound over three-dimensional ordered macroporous Ni–Pt/Ce1–xZrxO<sub>2</sub> catalysts. *Appl. Catal. A Gen.* **2020**, *607*, 117859. [[CrossRef](#)]
25. Silveira, E.B.; Rabelo-Neto, R.C.; Noronha, F.B. Steam reforming of toluene, methane and mixtures over Ni/ZrO<sub>2</sub> catalysts. *Catal. Today* **2017**, *289*, 289–301. [[CrossRef](#)]
26. Bengaard, H.S.; Nørskov, J.K.; Sehested, J.; Clausen, B.S.; Nielsen, L.P.; Molenbroek, A.M.; Rostrup-Nielsen, J.R. Steam Reforming and Graphite Formation on Ni Catalysts. *J. Catal.* **2002**, *209*, 365–384. [[CrossRef](#)]
27. Christensen, K.O.; Chen, D.; Lødeng, R.; Holmen, A. Effect of supports and Ni crystal size on carbon formation and sintering during steam methane reforming. *Appl. Catal. A Gen.* **2006**, *314*, 9–22. [[CrossRef](#)]
28. Sehested, J. Four challenges for nickel steam-reforming catalysts. *Catal. Today* **2006**, *111*, 103–110. [[CrossRef](#)]
29. Li, D.; Wang, L.; Koike, M.; Nakagawa, Y.; Tomishige, K. Steam reforming of tar from pyrolysis of biomass over Ni/Mg/Al catalysts prepared from hydrotalcite-like precursors. *Appl. Catal. B Environ.* **2011**, *102*, 528–538. [[CrossRef](#)]
30. Chen, X.; Tadd, A.; Schwank, J. Carbon deposited on Ni/CeZrO isooctane autothermal reforming catalysts. *J. Catal.* **2007**, *251*, 374–387. [[CrossRef](#)]
31. Bona, S.; Guillen, P.; Alcade, J.; Garcia, L.; Bilbao, R. Toluene steam reforming using coprecipitated Ni/Al catalysts modified with lanthanum or cobalt. *Chem. Eng. J.* **2008**, *137*, 587–597. [[CrossRef](#)]
32. Gould, B.D.; Chen, X.; Schwank, J.W. N-Dodecane reforming over nickel-based monolith catalysts: Deactivation and carbon deposition. *Appl. Catal. A Gen.* **2008**, *334*, 277–290. [[CrossRef](#)]
33. Kihlman, J.; Kaisalo, N.; Koskinen-Soivi, M.-L.; Simell, P.; Niemelä, M.; Lehtonen, J. Whisker carbon formation in catalytic steam reforming of biomass gasification gas. *Appl. Catal. B Environ.* **2018**, *564*, 133–141. [[CrossRef](#)]
34. Jin, Q.; Wang, A.; Lu, B.; Xu, X.; Shen, Y.; Zeng, Y. Steam reforming of formaldehyde for generating hydrogen and coproducing carbon nanotubes for enhanced photosynthesis. *Catal. Sci. Technol.* **2020**, *10*, 4436–4447. [[CrossRef](#)]
35. Quan, C.; Gao, N.; Wang, H.; Sun, H.; Wu, C.; Wang, X.; Ma, Z. Ethanol steam reforming on Ni/CaO catalysts for coproduction of hydrogen and carbon nanotubes. *Int. J. Energy Res.* **2019**, *43*, 1255–1271. [[CrossRef](#)]
36. Zhang, Y.; Williams, P.T. Carbon nanotubes and hydrogen production from the pyrolysis catalysis or catalytic-steam reforming of waste tyres. *J. Anal. Appl. Pyrolysis* **2016**, *122*, 490–501. [[CrossRef](#)]
37. Zhang, R.; Wang, B.; Tian, Y.; Ling, L. Quantum Chemistry Studies on the Free-radical Growth Mechanism of Polycyclic Arenes from Benzene Precursors. *Chin. J. Chem. Eng.* **2009**, *17*, 394–400. [[CrossRef](#)]
38. Tian, Y.; Hu, Z.; Yang, Y.; Chen, X.; Ji, W.; Chen, Y. Thermal analysis–mass spectroscopy coupling as a powerful technique to study the growth of carbon nanotubes from benzene. *Chem. Phys. Lett.* **2004**, *388*, 259–262. [[CrossRef](#)]

39. Tian, Y.; Hu, Z.; Yang, Y.; Wang, X.; Chen, X.; Xu, H.; Wu, Q.; Ji, W.; Chen, Y. In Situ TA-MS Study of the Six-Membered-Ring-Based Growth of Carbon Nanotubes with Benzene Precursor. *J. Am. Chem. Soc.* **2004**, *126*, 1180–1183. [[CrossRef](#)]
40. Feng, H.; Ma, J.; Hu, Z. Six-Membered-Ring-Based Radical Mechanism for Catalytic Growth of Carbon Nanotubes with Benzene Precursor. *J. Phys. Chem. C* **2004**, *113*, 16495–16502. [[CrossRef](#)]
41. Lee, D.C.; Mikulec, F.V.; Korgel, B.A. Carbon Nanotube Synthesis in Supercritical Toluene. *J. Am. Chem. Soc.* **2004**, *126*, 4951–4957. [[CrossRef](#)] [[PubMed](#)]
42. Bion, N.; Epron, F.; Duprez, D. Bioethanol reforming for H<sub>2</sub> production. A comparison with hydrocarbon reforming. In *Catalysis: Volume 22*; Spivey, J.J., Dooley, K.M., Eds.; RSC Publishing: London, UK, 2010; pp. 1–55, ISBN 9781847559517. [[CrossRef](#)]
43. Wang, X.; Gorte, R.J. A study of steam reforming of hydrocarbon fuels on Pd/ceria. *Appl. Catal. A Gen.* **2002**, *224*, 209–218. [[CrossRef](#)]
44. Doumani, T. Dealkylation of Organic Compounds. Benzene from Toluene. *Ind. Eng. Chem.* **1958**, *50*, 1677–1680. [[CrossRef](#)]
45. Xi, M.; Bent, B.E. Iodobenzene on Cu(111): Formation and coupling of adsorbed phenyl groups. *Surf. Sci.* **1992**, *278*, 19–32. [[CrossRef](#)]
46. Krishnankutty, N.; Rodriguez, N.M.; Baker, R.T.K. Effect of Copper on the Decomposition of Ethylene over an Iron Catalyst. *J. Catal.* **1996**, *158*, 217–227. [[CrossRef](#)]
47. Rodriguez, N.M. A review of catalytically grown carbon nanofibers. *J. Mater. Res.* **1993**, *8*, 3233–3250. [[CrossRef](#)]
48. Feng, H.; Qian, Z.; Wang, C.; Chen, C.; Chen, J. Theoretical investigation of formation mechanism of bipyridyl molecule on Ni(111) surface: Implication for synthesis of N-doped graphene from pyridine. *Phys. Chem. Chem. Phys.* **2011**, *13*, 6053–6058. [[CrossRef](#)]
49. Seemann, M.; Thunman, H. Methane synthesis. In *Substitute Natural Gas from Waste*; Academic Press: Cambridge, MA, USA, 2019; pp. 221–243. [[CrossRef](#)]
50. Hansen, H.A.; Wolverton, C. Kinetics and Thermodynamics of H<sub>2</sub>O Dissociation on Reduced CeO<sub>2</sub>(111). *J. Phys. Chem. C* **2014**, *118*, 27402–27414. [[CrossRef](#)]
51. Kim, S.; Merkle, R.; Maier, J. Oxygen nonstoichiometry of nanosized ceria powder. *Surf. Sci.* **2004**, *549*, 196–202. [[CrossRef](#)]
52. Kundakov, L.; Mullins, D.R.; Overbury, S.H. Adsorption and Reaction of H<sub>2</sub>O and CO on Oxidized and Reduced Rh/CeO<sub>x</sub>(111) Surfaces. *Surf. Sci.* **2000**, *457*, 51–62. [[CrossRef](#)]
53. Chen, B.; Ma, Y.; Ding, L.; Xu, L.; Wu, Z.; Yuan, Q.; Huang, W. Reactivity of Hydroxyls and Water on a CeO<sub>2</sub>(111) Thin Film Surface: The Role of Oxygen Vacancy. *J. Phys. Chem. C* **2013**, *117*, 5800–5810. [[CrossRef](#)]
54. Henderson, M.A.; Perkins, C.L.; Engelhard, M.H.; Thevuthasan, S.; Peden, C.H.F. Redox Properties of Water on the Oxidized and Reduced Surfaces of CeO<sub>2</sub>(111). *Surf. Sci.* **2003**, *526*, 1–18. [[CrossRef](#)]
55. Carrasco, J.; López-Durán, D.; Liu, Z.; Duchoñ, T.; Evans, J.; Senanayake, S.D.; Crumlin, E.J.; Matolín, V.; Rodríguez, J.A.; Ganduglia-Pirovano, M.V. In Situ and Theoretical Studies for the Dissociation of Water on an Active Ni/CeO<sub>2</sub> Catalyst: Importance of Strong Metal-Support Interactions for the Cleavage of O-H Bonds. *Angew. Chem. Int. Ed.* **2015**, *54*, 3917–3921. [[CrossRef](#)]